Check for updates

Received: 1 October 2022 | Revised: 21 December 2022 | Accepted: 21 December 2022

DOI: 10.1111/jace.18979

Journal of the American Ceramic Society

RESEARCH ARTICLE

Ab initio study of boron-rich amorphous boron carbides

Tevhide Ayça Yıldız | **Murat Durandurdu**

Materials Science and Mechanical Engineering Program and Department of Nanotechnology Engineering, Abdullah Gül University, Kayseri, Turkey

Correspondence
Murat Durandurdu, Materials Science and Mechanical Engineering Program and Department of Nanotechnology Engineering, Abdullah Gül University, Kayseri 38080, Turkey.
Email: murat.durandurdu@agu.edu.tr

Funding information
Scientific and Technological Research Council of Turkey, Grant/Award Number: 117M372; YÖK, Grant/Award Number: 100/2000; TÜBİTAK BİDEB, Grant/Award Number: 2211-C

Abstract

Amorphous boron carbide compositions having high B contents (B_xC_{1-x}, $0.50 \leq x \leq 0.95$) are systematically created by way of ab initio molecular dynamics calculations, and their structural, electrical, and mechanical characteristics are inclusively investigated. The coordination number of both B and C atoms increases progressively with increasing B/C ratio and more close-packed materials having pentagonal pyramid motifs form. An amorphous diamond-like local arrangement is found to be dominant up to 65% B content, and beyond this content, a mixed state of amorphous diamond– and B-like structures is perceived in the models because sp^3 hybridization around C atoms is still leading one for all compositions. The pentagonal pyramid motifs around C atoms are anticipated to appear beyond 65% content. The intericosahedral linear C–B–C chains do not form in any model. All amorphous boron carbides are semiconducting materials. The mechanical properties gradually increase with increasing B concentration, and some amorphous compositions are proposed to be hard materials on the basis of their Vickers hardness estimation.

KEYWORDS
amorphous, boron carbide, boron-rich, first-principles calculations, mechanical properties

1 | INTRODUCTION

Boron (B), carbon (C), or nitrogen (N) compounds form covalently bonded solids, and they are recognized as hard materials.[1] One of which is boron carbide[2–4] and is a semiconducting system possessing a wide bandgap depending on the B-to-C stoichiometry.[5,6] Boron carbide compounds are promising materials for several high-technology industries due to their distinguished features, such as good chemical inertness, high hardness, low wear coefficient, high melting point, and low density.[7–12] Because of their unique electronic properties,[8,13] they can have applications in photovoltaic and beta-voltaic devices,[8,14] diodes and transistors,[7] and neutron detectors[15–19] as well. In addition, combining their attractive properties such as lightweight and high hardness, they can be also used in body armor applications.[7,20,21]

The first boron carbide material was synthesized in 1858. However, it was not attained enough consideration until 1934.[22] The stoichiometric ratio as B_4C was studied in the mid-1930s.[23] Up to date, boron carbide with different B/C ratios has been fabricated using numerous experimental procedures, such as plasma-enhanced chemical vapor deposition,[24] magnetron sputtering,[3,4,25,26] pulsed laser deposition,[27–29] ion beam synthesis,[30] hot pressing, and spark plasma sintering.[31–33]

The atomic structure and mechanical characteristics of boron carbide materials appear to be relatively sensitive to B/C ratios. The studies proposed that B substation first modified C atoms in the $B_{11}C$ icosahedra transforming $B_{11}C$ to B_{12} molecules, and then excess B atoms revised C–B–C chains.[31] For the B/C < 4 materials, on the other hand, the existence of free C atoms in the microstructure and the formation of B_4C- and graphite-like structures

 © 2023 The American Ceramic Society.

at a C concentration of >20 at.%. were suggested.[32] As expected, the change in the local structure has obvious impacts on the mechanical properties of boron carbide. The maximum fracture toughness and hardness were observed for the stoichiometric composition (B_4C), and they surprisingly decreased for nonstoichiometric B_4C ($B/C > 4$ and $B/C < 4$) compositions.[34] For $B/C > 4$ materials, the decrease was attributed to the weakening of the bond strength (substitution of the stronger B–C bonds with weaker B–B bonds), whereas the decrease for $B/C < 4$ compositions was dedicated to free C atoms in the microstructure.[34]

Amorphous state of boron carbides has also drawn attentions due to their unique properties and has been considered both experimentally and theoretically.[15,35,36] An experimental investigation confirmed that pentagonal pyramids were the most preferable clusters in amorphous B_4C (a-B_4C).[35] The atomic and electronic behaviors of a-B_4C were investigated at the ab initio level using two different systems (containing 120 and 135 atoms), and several important findings were exposed. This computational study proposed that both amorphous configurations consisted of a random icosahedral network without linear chains, and a-B_4C owned a semimetal character.[15] Later, the combination of experimental and theoretical studies provided valuable information regarding the local structure of a-$B_{2.5}C$ and revealed that it consisted of B_{12}, $B_{11}C$, and $B_{10}C_2$ icosahedrons.[36]

Hydrogenated amorphous boron carbide films having several B/C ratios[37,38] were also prepared. The basis of these studies is about their compositional, structural, physical, electrical–optical, and mechanical properties. a-$B_xC{:}H_y$ thin films ($3.4 \leq B/C \leq 4.9$ and H concentration changing from 10% to 45%) were fabricated via the PECVD technique, and they were found to have density from 0.9 to 2.3 g/cm^3, Young's modulus from 10 to 340 GPa, and bandgap between 1.7 and 3.8 eV.[37] In a different investigation, a-$B_xC{:}H_y$ thin films ($3.4 \leq B/C \leq 4.9$ and H content varying from 37.5% to 50.5%) were synthesized by the PEVCD process, and it was proposed that the thin films had a good thermal conductivity (0.31 ± 0.03 W/(m K) and the Young modulus of 12 ± 3 GPa.[38]

Although there have been some investigations on the microstructure and mechanical descriptions of B-rich boron carbides, there is no elaborated information about the structural, electrical, and mechanical features of their amorphous form(s). In the current study, possible B-rich amorphous boron carbides with 10 different B/C ratios (B_xC_{1-x}, $0.50 \leq x \leq 0.95$) are modeled via ab initio molecular dynamics (MD) simulations, and some important properties (structural, electrical, and mechanical) are exposed in detail.

2 | COMPUTATIONAL METHOD

All calculations were executed by using the SIESTA ab initio code[39] within a pseudopotential method[40] and a generalized gradient approximation (GGA) proposed by Becke gradient exchange functional[41] and Lee et al. correlation functional.[42] A double-zeta was adopted as the atomic orbital basis set for the valence electrons. The grid mesh cutoff was set to 120 Ry, and the Γ-point sampling of *k*-mesh was applied for the Brillouin zone integration. The time step was selected as 1 femtosecond (fs). All simulations were done within the NPT (constant number of atoms, constant pressure, and constant temperature) ensemble. The controlling of temperature and pressure was managed by the velocity scaling and the Parrinello–Rahman[43] techniques, correspondingly. We used a BN melt consisting of 200 atoms as an initial structure and replaced all N atoms with C atoms. Later, the structure was equilibrated at 3400 K for 40 picoseconds (ps). To achieve a definite amount of B concentration (55%–95%), C atoms were randomly replaced by B atoms. Depending on B content, then each configuration was explored to 3400 K (50 at.% B) −2500 K (95 at.% B) for 40 ps in order to get a well-equilibrated melt, and then the melts were quenched to 300 K in ∼155–110 ps. Eventually, the resulting structures at 300 K were relaxed via a conjugate gradient technique until the maximum force was less than 0.02 eV/Å. In the present study, the density of c-B_4C is estimated to be about 2.45 g/cm^3, fairly parallel to 2.52 g/cm^3.[36] On the other hand, the density of amorphous materials ranges from ∼1.97 to 2.24 g/cm^3, less than 2.47 (±0.01) g/cm^3 reported for a-$B_{2.5}C$ in an experimental study.[36] The VESTA[44] program for the visualization of the random structures was used. Figure 1 reveals the ball stick demonstration of some selected amorphous arrangements.

3 | RESULTS

3.1 | Local structure

The partial pair distribution functions (PPDFs) investigation is one of the effective schemes to offer valuable descriptions about the characteristic of a structure at the atomistic level. Figure 2 shows the PPDFs of some amorphous boron carbide configurations. There are some notable changes in the distributions with changing B content as expected. As the B/C ratio increases, the intensity of the first and, similarly, second B–B peaks increases, due to the formation of more pentagonal pyramid-like motifs. For the B–C pairs, the intensity of the first peak moderately

15512916, 2023, 5, Downloaded from https://ceramics.onlinelibrary.wiley.com/doi/10.1111/jace.18979 by Abdullah Gul University, Wiley Online Library on [01/04/2024]. See the Terms and Conditions (https://onlinelibrary.wiley.com/terms-and-conditions) on Wiley Online Library for rules of use; OA articles are governed by the applicable Creative Commons License

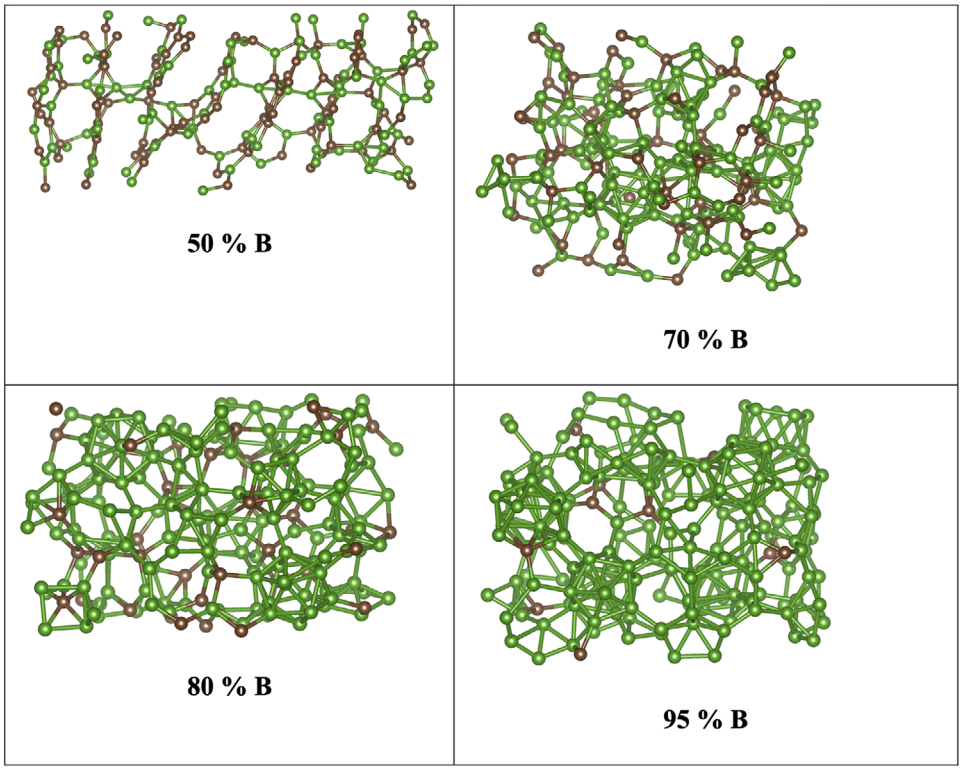

FIGURE 1 Ball stick representation of some amorphous models

decreases with increasing B content. C–C bonds exist only between 50% and 80% B concentrations.

The first peak position of PPDFs can be used to determine the mean bond separation for each pair. The average B–B bond length has the values of 1.75–1.77 Å, indicating that B content has almost no effect on this bonding. The range perceived is reasonably coherent with previously reported data of 1.75 Å in a-$B_{2.5}C$,[36] 1.74–1.80 Å in c-B_4C,[45] and 1.73–1.80 Å formed in the liquid, amorphous, and crystalline phases of B.[46–48] The mean B–C bond distance is estimated to be 1.55–1.58 Å. Again, it appears that B content does not have a significant impact on this bonding as well. Our B—C estimations are also comparable with 1.57 Å in a-$B_{2.5}C$,[36] 1.64 Å in c-B_4C,[45] and 1.60 Å in c-$B_{13}C_2$.[49] The C–C bond distance is predicted to be in the range of 1.43–1.56 Å, which are comparable with 1.54 Å reported for a-$B_{2.5}C$,[36] 1.39–1.45 Å in c-B_4C,[45] 1.42 Å in graphite, and 1.54 Å in diamond.[50] Relative to the other separations, C–C bond seems to be sensitive to B content, which is probably correlated with the formation of different motifs (from threefold to sixfold coordinated) around C atoms having homopolar bonds.

In order to validate our results, we compare atomic structure factor $S(Q)$ and reduced pair distribution function $G_{PDF}(r)$ of two compositions [a-$B_{70}C_{30}$ and a-$B_{75}C_{25}$] with the neutron diffraction data of a-$B_{2.5}C$[36] and provide them in Figure 3. One can see that in spite of the small size of simulation boxes and different composition ratios, our results fairly agree with the experiment.

The total and partial coordination numbers (CNs) are positively needed to shed some light onto the local structure of a material at the atomistic level, and hence, in the second step, we estimate them by way of cutoff distances (the first minimum) of PPDFs (2.04–2.33 Å for the B–B correlation, 2.10–2.17 Å for the B—C distribution and 1.91–2.07 Å for the C—C pairs depending upon B concentration). As shown in Figure 4, the average CN of B atoms increases continuously from 3.22 to 5.70, whereas that of C atoms changes steadily from 3.46 to 4.30. As we will discuss below, B atoms have a strong tendency to form sixfold-coordinated pentagonal pyramid-like motifs. As B content increases, more B atoms are able to form sixfold-coordination, and hence, the mean CN of B atoms gradually increases. We also see the development of pentagonal pyramid-like motifs around some C atoms (see the Voronoi analysis below) as in c-B_4C[51] and a-$B_{2.5}C$.[36] Thus, such a development leads to high mean coordination for C atoms. We specifically focus on the 80% B content because it is a well-studied material and find the mean CN of a-B_4C to be 4.15, which is comparable with 4.66 in c-B_4C.

In order to have more knowledge on the atomic structure of the networks, the coordination distribution is considered and provided in Figure 5. As seen from the figure,

15512916, 2023, 5, Downloaded from https://ceramics.onlinelibrary.wiley.com/doi/10.1111/jace.18979 by Abdullah Gul University, Wiley Online Library on [01/04/2024]. See the Terms and Conditions (https://onlinelibrary.wiley.com/terms-and-conditions) on Wiley Online Library for rules of use; OA articles are governed by the applicable Creative Commons License

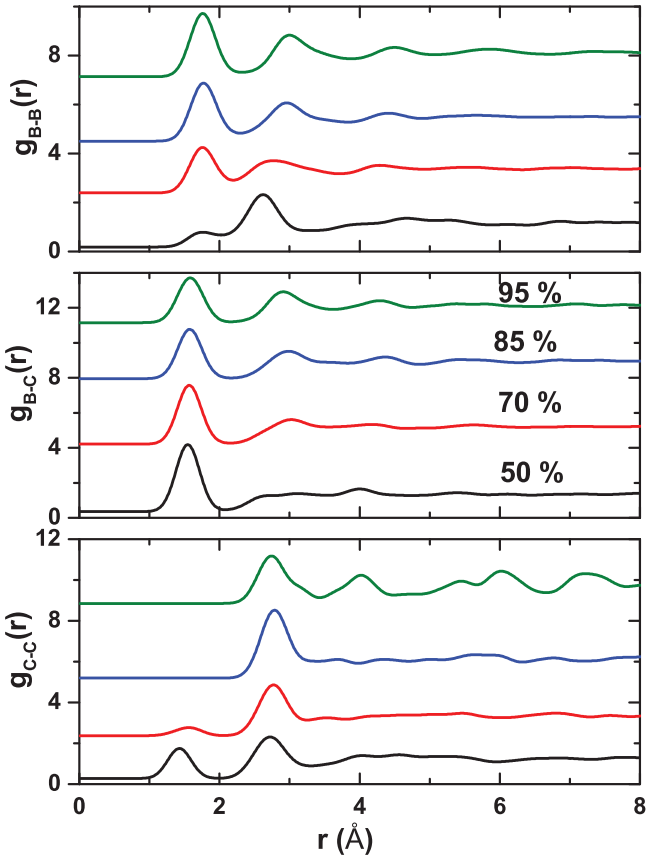

FIGURE 2 Partial pair distribution functions of some B concentrations

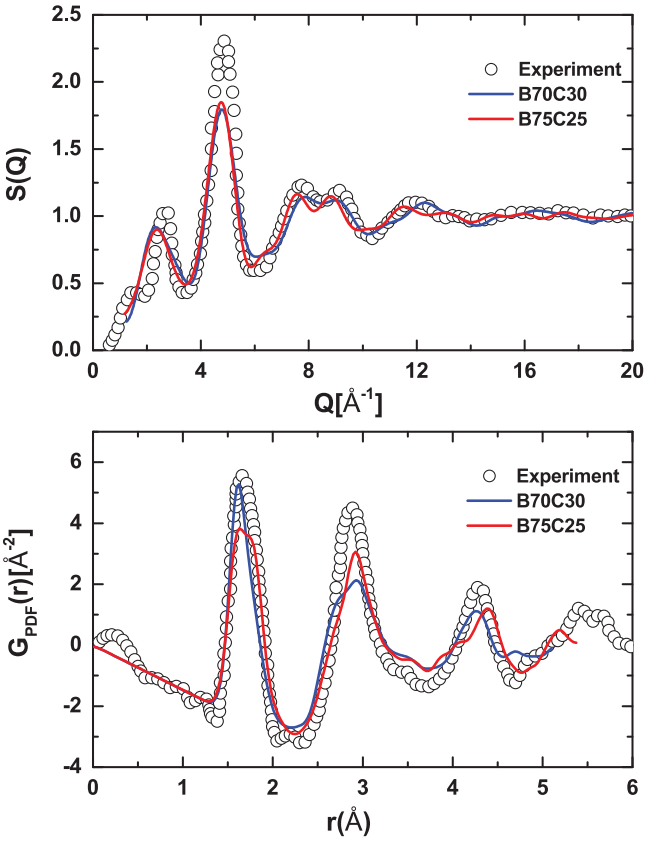

FIGURE 3 Comparison of atomic structure factor $S(Q)$ and reduced pair distribution function $G_{PDF}(r)$ of two compositions [a-$B_{70}C_{30}$ and a-$B_{75}C_{25}$] with the neutron diffraction data of a-$B_{2.5}C$. *Source*: The experimental data are extracted from Ref. [36]

threefold-coordinated B atoms, supporting sp^2 hybridization, are prevailing at 50% B concentration and quickly decrease with increasing B content, whereas the sixfold-coordination rapidly increases. Fourfold-coordination, on the other hand, remains almost null up to 80% at which point it starts to decrease. Fivefold-coordination becomes noticeable at 60 at.% B and remains practically unchanged thereafter. Sevenfold-coordination develops at 65% B concentration, and its fraction reaches a maximum value of 17%. On the other side, for C atoms, threefold- and fourfold-coordinated structures with a fraction of 56% and 42%, respectively, are dominant at 50 at.% B. With the increase of B content, threefold-coordination decreases drastically, and parallel to this decrease, fourfold-coordination increases initially, remains nearly unaffected between 60% and 85% B contents, and then begins to decrease again. Fivefold-coordinated configuration gradually increases from 2% to 30%. Sixfold-coordinated motif first develops at 70% B content and reaches a maximum value of 10% at 90 at.% B.

The bond angle distribution function analysis is performed to provide further information on the microstructure of amorphous boron carbide configurations. Figure 6 shows the B–B–B, B–C–B, C–B–C, and C–C–C bond angle distributions of some amorphous models. The B—B—B angles possess a wide distribution with several peaks ranging from roughly 56° to 122° because of twofold-to-fivefold structures, respectively, at 50% B concentration. From 70% to 95% B content, the distribution has two clear peaks at roughly 60° and 107°, which are indeed related to intra-icosahedral bonds of the pentagonal pyramids. The B—C—B angles show a broad distribution nearly from 62° to 148° owing to forming of the different types of C motifs between 50% and 65% B contents. After 70% B range, the first peak is placed at about 109° in view of tetrahedral angle, whereas the second peak is due to the B–C–B zigzag-like motifs, and it shifts from 114° to 121° with increasing B concentration. On the account of the existence of hexagonal angles in the disordered networks, the C—B—C distribution has a moderate peak at around 120° at 50%–70% B concentrations. With increasing B content, the main peaks are sharpened, especially at 95% B content, at nearly 115° and 128°, resulting from a structure like a bridge between incomplete pentagonal pyramids. The C—C—C angles of 50% B content possess two clear peaks at about 109° and 120° related to ideal tetragonal

15512916, 2023, 5, Downloaded from https://ceramics.onlinelibrary.wiley.com/doi/10.1111/jace.18979 by Abdullah Gul University, Wiley Online Library on [01/04/2024]. See the Terms and Conditions (https://onlinelibrary.wiley.com/terms-and-conditions) on Wiley Online Library for rules of use; OA articles are governed by the applicable Creative Commons License

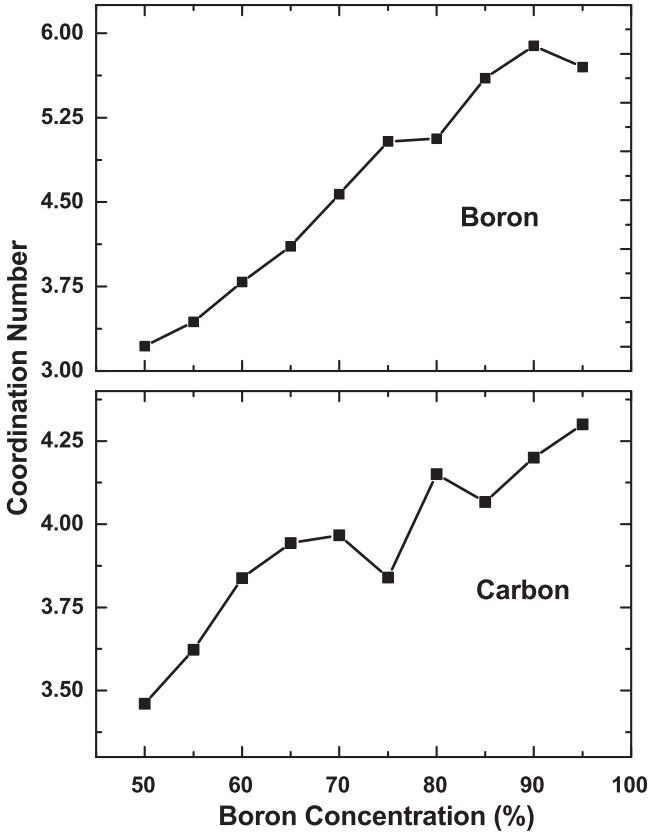

FIGURE 4 Modification of partial coordination numbers as a function of B concentration

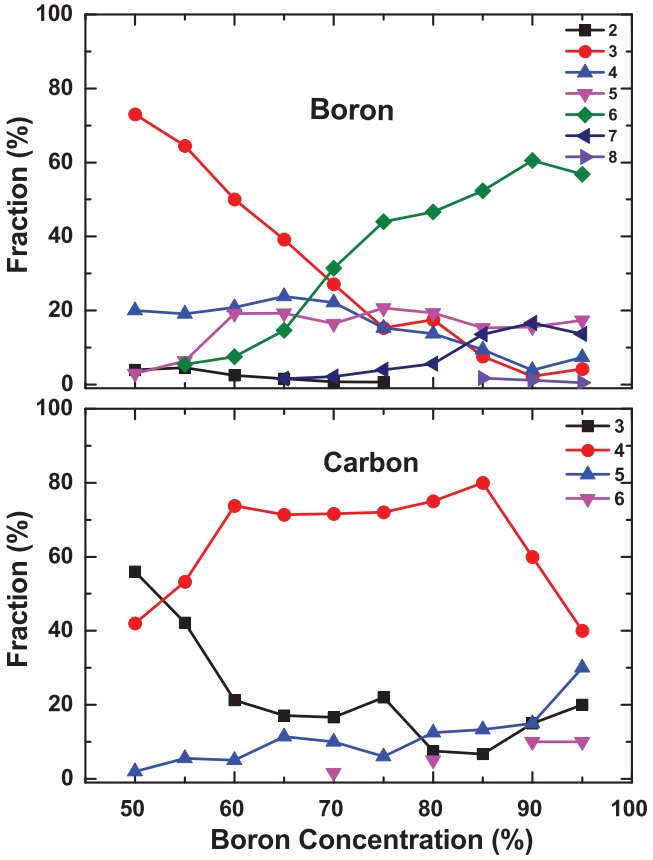

FIGURE 5 Coordination distribution of B and C atoms as a function of B concentration

and hexagonal angles, respectively. At 70% B concentration, there is a sharp peak at around 112°. The origin of this peak comes from the threefold-coordinated structure similar to zigzag shape formed by only three C atoms. And lastly, two apparent peaks of the C—C—C angle distribution function are placed at around 120° and 131° at 75% B content.

The Voronoi polyhedral method[52] is a powerful tool to examine the kind of clusters formed around an atom. According to this approach, a polyhedron is notated via several Voronoi indices $<n_3, n_4, n_5, n_6>$, where n_i and $\sum n_i$ represent the number of i-edge faces of a cluster and its total CN, correspondingly. It is known that the main structure of ordered and disordered forms of B and B-rich materials consists of quasimolecular B_{12} icosahedron that involves ideal pentagonal pyramids. Consequently, in order to further understand the microstructure of the amorphous models as well as to define the geometrical structures, the Voronoi polyhedral approach is used. For this analysis, we concentrate mainly on <2,2,2,0> and <2,3,0,0> indices, presenting ideal and defective pentagonal pyramid-like geometries. Figure 7 displays their alternation as a function of B concentration. For B atoms, as the B concentration increases, the fraction of <2,2,2,0> type polyhedron raises from 5% to 55%. The frequency of <2,3,0,0> geometry alters from 3% to 16%. These analyses suggest that, as expected, the ideal and defective pentagonal pyramid-like geometries develop around B atom. As for C atoms, the frequency of <2,2,2,0> type motif begins to form at 70% B content, and its maximum fraction is 10%. The portion of <2,3,0,0> structure ranges from 2% to 30%. The examination discloses that some C atoms have a tendency to form pyramid-like structures in amorphous boron carbides as well.

3.2 | Electronic properties

B compounds might possess the electronic structure such that they can offer some potential applications such as diodes and thermocouple consisting transistors, and thus, the analyzing of electronic properties of amorphous networks generated is mandatory in this study. We first focus on c-B_4C and found that its bandgap defined as a difference between HOMO and LUMO state is nearly 2.9 eV based on the GGA calculation (Figure 8), comparable well with 2.6–3.0 eV[15,53–56] predicted in the earlier DFT-GGA/LDA

15512916, 2023, 5, Downloaded from https://ceramics.onlinelibrary.wiley.com/doi/10.1111/jace.18979 by Abdullah Gul University, Wiley Online Library on [01/04/2024]. See the Terms and Conditions (https://onlinelibrary.wiley.com/terms-and-conditions) on Wiley Online Library for rules of use; OA articles are governed by the applicable Creative Commons License

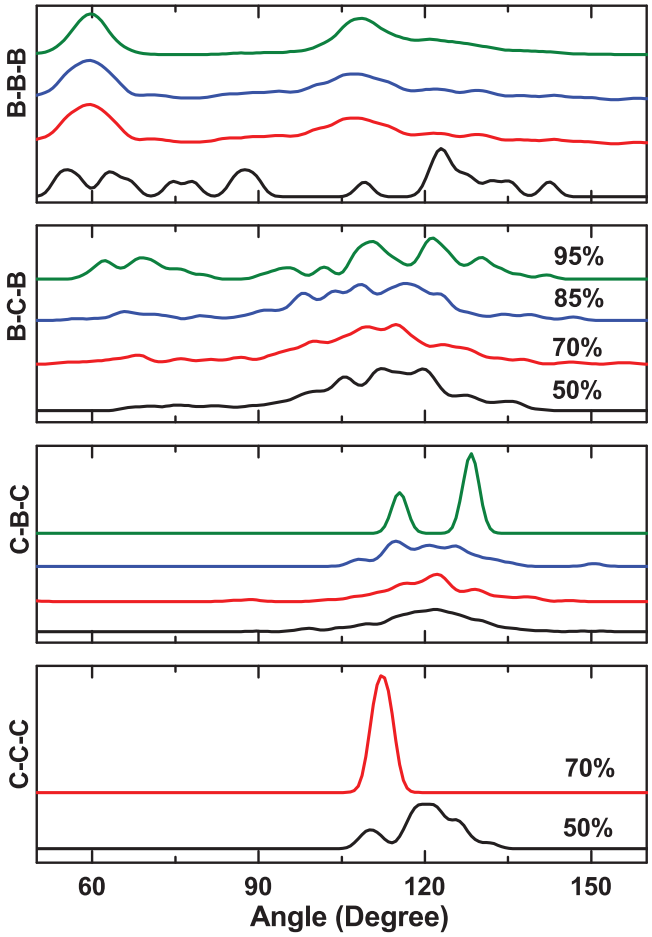

FIGURE 6 Bond angle distribution functions at some B concentrations

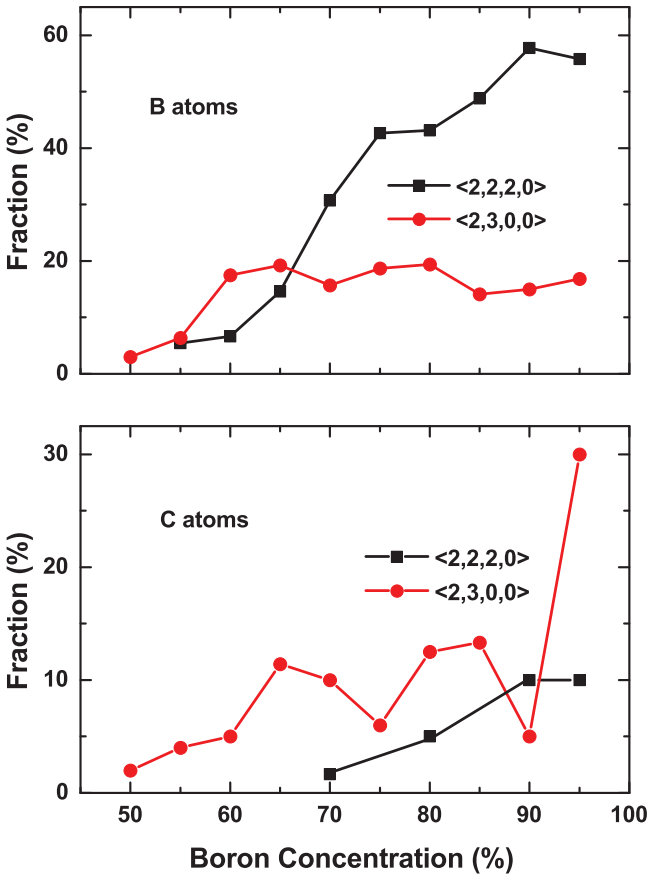

FIGURE 7 Fraction of ideal (<2,2,2,0>) and defective (<2,3,0,0>) pentagonal pyramids

studies but less than 3.84 eV based on a DFT-hybrid exchange functional (HEF) calculation.[57] In order to estimate more accurate bandgap energy of the amorphous states, we perform GGA + U calculations by taking the DFT–HEF estimation as our reference. We change the Hubbard potential U (for B-p states because they are more dominant near the Fermi level for both valence and conduction bands) until the bandgap energy of c-B_4C is close to the DFT–HEF prediction of 3.84 eV.[57] We find that U = 4.5 eV (for B-p state) yields a bandgap of 3.85 eV for c-B_4C in our calculation, and the same U is used for all amorphous configurations. The forbidden bandgap of the amorphous models shows an increasing trend with increasing B content and is in the range of 0.2–1.47 eV as shown in Figure 8. It should be noted here that some mid-gap states near the Fermi level are observed for some amorphous configurations such that their bandgap is projected by ignoring them. Considering the disordered nature of the models, one can see that our predictions are objectively comparable with the values of 0.77–1.80 eV in the crystals with B/C = 2.4–50.[58]

3.3 | Mechanical properties

The mechanical descriptions, including the bulk modulus, Poisson's ratio, Young modulus, shear modulus, Vickers hardness, and Pugh's ratio, are vital to the applications of a material in technology. Therefore, the mechanical features of the amorphous models are inclusively investigated. For comparison purposes, Table 1 gives the mechanical properties of some B concentrations in this study along with the data of some related crystal and amorphous materials in the literature.

The bulk moduli (K), the compressibility of a material under pressure, are calculated by fitting the energy–volume relation of each model to the third-order Birch–Murnaghan equation of states:

$$E\ (V) = E_0 + \frac{9V_0K}{16}\left\{\left[\left(\frac{V_0}{V}\right)^{2/3} - 1\right]^3 K' + \left[\left(\frac{V_0}{V}\right)^{2/3} - 1\right]^2 \left[6 - 4\left(\frac{V_0}{V}\right)^{2/3}\right]\right\} \quad (1)$$

15512916, 2023, 5, Downloaded from https://ceramics.onlinelibrary.wiley.com/doi/10.1111/jace.18979 by Abdullah Gul University, Wiley Online Library on [01/04/2024]. See the Terms and Conditions (https://onlinelibrary.wiley.com/terms-and-conditions) on Wiley Online Library for rules of use; OA articles are governed by the applicable Creative Commons License

TABLE 1 The mechanical properties of some B concentrations in this study along with the data of some crystal and amorphous materials in the literature

	K (GPa)	*E* (GPa)	μ (GPa)	*ν*	*H* (GPa)	References
a-$B_{50}C_{50}$	105	142	56	0.27	~7–9	This study
g-graphite	38					59
				0.28		67
		23–32	10–13		~2–3	70
Graphite				0.27		68
Amorphous C[a]		40–145		0.25	~5–15	69
a-$B_{80}C_{20}$	170	288	120	0.22	~18	This study
a-B_4C		255–351			~21–34	71
c-B_4C	245	470	200	0.17	~30–32	This study
c-B_4C	248–274	441–472	188–200	0.17–0.18		51, 61–64, 73, 78
					~45	63
					~42	71
a-$B_{85}C_{15}$	193	326	135	0.21	~20	This study
c-$B_{85}C_{15}$			195–197	0.17		62
	245	466	197	0.18		65
a-$B_{90}C_{10}$	199	370	155	0.19	~23–25	This study
c-$B_{90}C_{10}$	130–183	319–348		0.16–0.21		62
	170–194	323–348	132–150	0.16–0.22		65
a-$B_{95}C_5$	183	332	139	0.20	~20–23	This study
a-B		320				72
γ-B	224		236	0.11		66

Abbreviation: g-graphite, glassy graphite.
[a]With different sp^3/sp^2 ratios.

where E and E_0 stand for the energy and the equilibrium energy, correspondingly, whereas V and V_0 represent the volume and the equilibrium volume, respectively. K' is the derivative of K with respect to pressure ($K' = dK/dP$). Figure 9 represents the change in K as a function of B content. As can be seen from the figure, it gradually increases. a-$B_{50}C_{50}$ has a value of nearly 105 GPa. The comparison with glassy graphite (g-graphite) ($K = 38$ GPa)[59] suggests that a-$B_{50}C_{50}$ shows better incompressibility relative to g-graphite, but it is considerably less than 363 GPa in the diamond-like amorphous carbon.[60] For c-B_4C, our estimation is 245 GPa, comparable with the previous data of 248–274 GPa.[51,61–64] On the other hand, its amorphous form has a value of 170 GPa, suggesting a noticeable softening by amorphization. Similar trend is also observed for 85% B concentration; namely, the bulk modulus of a-$B_{85}C_{15}$ ($K = 193$ GPa) is again smaller than 245 GPa in its crystalline form.[65] The K value of a-$B_{90}C_{10}$, about 199 GPa, is larger than 130–183[62] and 170–194 GPa[65] in its crystalline counterpart. For a-$B_{95}C_5$, it is computed to be nearly 183 GPa. Because there is no data available in the literature for this composition, we compare it with a crystalline B phase (*γ*-B), the K of which is 224 GPa.[66] One can see that amorphization causes a visible decrease in bulk modulus.

Poisson's ratio (ν), described as the ratio of transverse strain to longitudinal strain computed by the application of a uniaxial strain along the principal axes, is estimated using the following equation:

$$\nu_{ij} = -\frac{\Delta L_i/L_i}{\Delta L_j/L_j} \quad (2)$$

where L_s are the magnitude of the supercell's vectors, and i and j represent the principal (x, y, and z) directions. As shown in Figure 9, ν decreases with increasing B content and lies in the range of nearly 0.27–0.20. For a-$B_{50}C_{50}$, it is found to be roughly 0.27, which rather well overlaps with 0.28, 0.27, and 0.25 reported for g-graphite, graphite, and amorphous carbon with different sp^3/ sp^2 ratios,[67–69] respectively. For c-B_4C, our calculation is 0.17, quite coherent with the experimental data of 0.17 and 0.18.[61–63] On the other side, for a-B_4C, ν is about 0.22 and slightly higher than that of c-B_4C[61–63] due to its amorphous nature. ν is 0.21 for a-$B_{85}C_{15}$, whereas its crystalline counterpart has the values of 0.17–0.18.[62,65] For a-$B_{90}C_{10}$, the ratio is about 0.19, parallel to 0.16–0.22 in c-$B_{90}C_{10}$.[62,65]

Young modulus (E), in other words, elastic modulus, stiffness of the material, is characterized with relationship

15512916, 2023, 5, Downloaded from https://ceramics.onlinelibrary.wiley.com/doi/10.1111/jace.18979 by Abdullah Gul University, Wiley Online Library on [01/04/2024]. See the Terms and Conditions (https://onlinelibrary.wiley.com/terms-and-conditions) on Wiley Online Library for rules of use; OA articles are governed by the applicable Creative Commons License

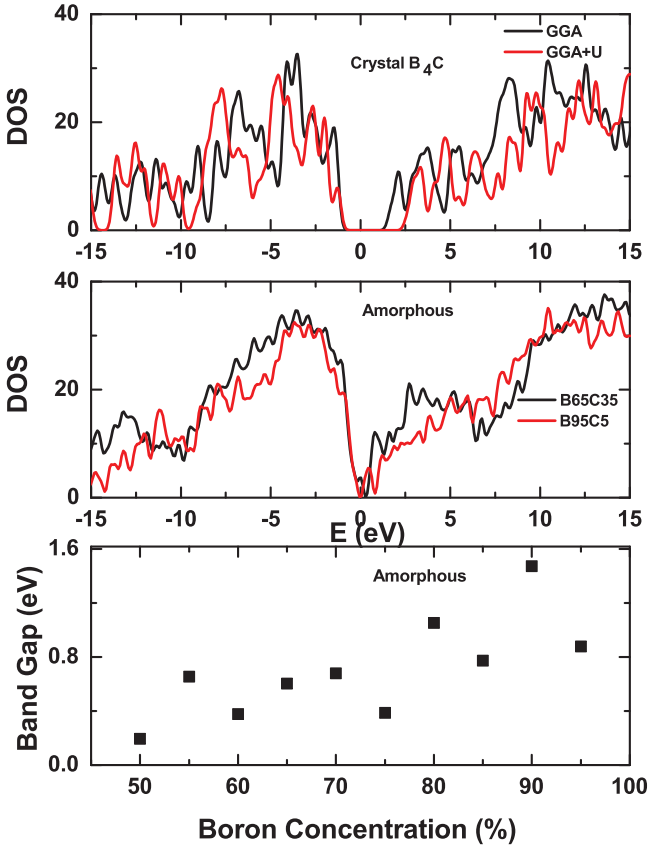

FIGURE 8 The bandgap energy of B_4C crystal (top panel). The bandgap energy of amorphous forms of $B_{65}C_{35}$ and $B_{95}C_5$ (middle panel). Variation of bandgap energy of amorphous materials as a function of B content (bottom panel)

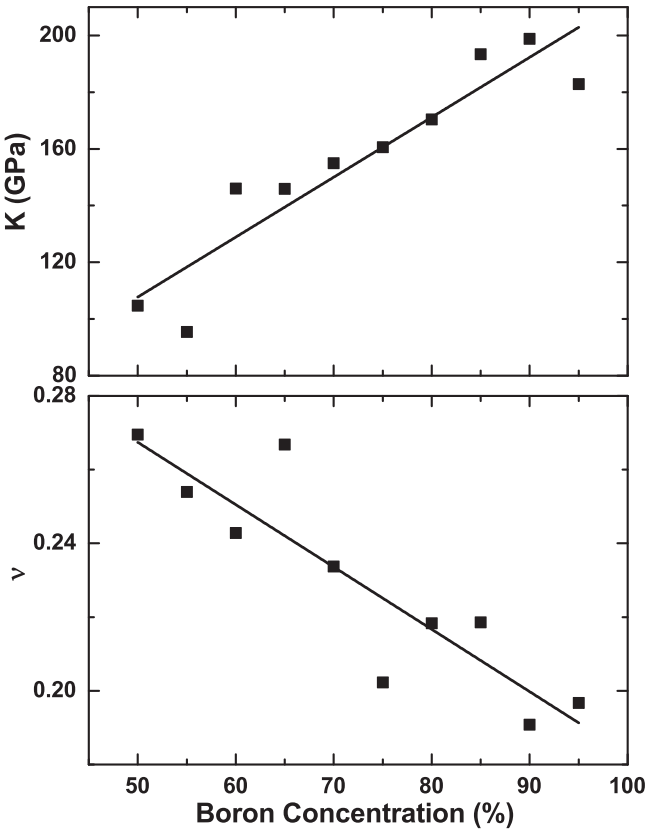

FIGURE 9 Variation of Bulk modulus (K) and Poisson's ratio (ν) as a function of B content

between stress and strain in a material under a uniaxial deformation. E is related to both K and ν values and is practically obtained by the way of the following equation:

$$E = 3K\ (1 - 2\nu) \tag{3}$$

The Young modulus computed increases gradually from about 140 to 370 GPa with increasing B content as seen in Figure 10. For a-$B_{50}C_{50}$, E is projected to be about 142 GPa, whereas it is 23–32 GPa for g-graphite,[70] meaning that this material is more stiffer than g-graphite. However, in an earlier study on amorphous carbon with different sp^3/ sp^2 ratios,[69] E is reported as 40–145 GPa, which is parallel to our result for a-$B_{50}C_{50}$. For c-B_4C, E is estimated to be 470 GPa, and it is pretty akin to the previously reported values of 441–472 GPa.[61,62,73,78] E is nearly 288 GPa in a-B_4C, and it is comparable with experimental values of 255–351 GPa in a-B_4C.[71] When a-$B_{85}C_{15}$ is concerned, E is about 326 GPa, noticeably less than 466 GPa[66] in its crystalline form. a-$B_{90}C_{10}$ has the highest value of 370 GPa, as seen in Table 1, in a good agreement with 319–348[62] and 323–348 GPa[65] in c-$B_{90}C_{10}$. E is ~332 GPa for a-$B_{95}C_5$, which is close to the experimental measurement of 320 GPa in a-B.[72] Eventually, the higher the B content, the stiffer the amorphous material forms.

Shear modulus (μ), the ability to resist shear deformation, can be defined as the ratio of shear stress to the shear strain of the material within the restricted elastic deformation and can be achieved by using the following definition:

$$\mu = \frac{E}{2\ (1 + \nu)} \tag{4}$$

As can be seen from Figure 10, μ exhibits a similar behavior with K and E. With increasing B content, μ progressively changes from ~56 to 155 GPa. For a-$B_{50}C_{50}$, μ is computed as 56 GPa, which is quite higher than 10–13 GPa in g-graphite,[70] implying that it shows more resistance to shear deformation, relative to g-graphite. The calculated μ of a-B_4C is about 120 GPa, whereas the estimated μ value for c-B_4C is nearly 200 GPa. Our results, especially for crystalline form, are rather close to the previous results of about 188–200 GPa.[61,62,73] Similarly, a noticeable decrease in μ is observed for $B_{85}C_{15}$ composition: It is about 135 GPa in a-$B_{85}C_{15}$ and 195–197 GPa in c-$B_{85}C_{15}$.[62,65] On the other hand, μ is projected as 155 GPa for a-$B_{90}C_{10}$, comparable with

15512916, 2023, 5, Downloaded from https://ceramics.onlinelibrary.wiley.com/doi/10.1111/jace.18979 by Abdullah Gul University, Wiley Online Library on [01/04/2024]. See the Terms and Conditions (https://onlinelibrary.wiley.com/terms-and-conditions) on Wiley Online Library for rules of use; OA articles are governed by the applicable Creative Commons License

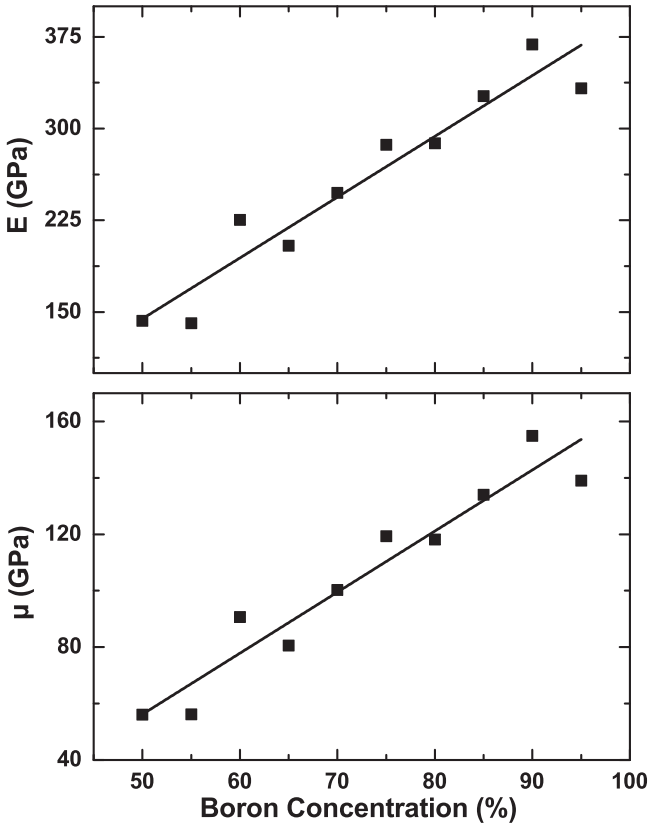

FIGURE 10 Variation of Young's modulus (E) and shear modulus (μ) as a function of B content

132–150 GPa in c-$B_{90}C_{10}$.[65] Consequently, one can see that the estimated μ values are roughly equal to or less than that of their crystalline counterparts.

Vickers hardness (H_v), a measure of the resistance of a material to deformation, can be useful to determine the correlation between hardness and elastic properties. H_v can be approximately projected by different practical correlations related to various mechanical properties of a material such as μ and E[74–77]:

$$H_v = 0.151\mu \quad (5)$$

$$H_v = 2\left(\frac{\mu}{n^2}\right)^{0.585} - 3 \text{ (GPa)} \quad (6)$$

$$H_v = 0.92\left(\frac{1}{n}\right)^{1.137}(\mu)^{0.708} \quad (7)$$

$$H_v = 0.0635E \quad (8)$$

The alteration of the hardness is illustrated in Figure 11, and it rises from ~7 to 25 GPa with increasing B concentration. The computed H_v value for a-$B_{50}C_{50}$ is in the range of 7–9 GPa, as given in Table 1, apparently higher than 2–3 GPa in g-graphite[70] but relatively closer to 5–15 GPa in amorphous carbon having different sp^3/sp^2 ratios.[69] H_v is projected to be 18 GPa for a-B_4C, whereas it is reported

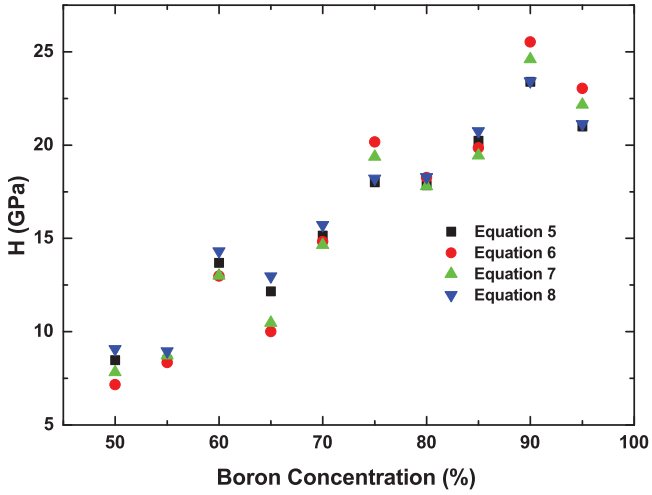

FIGURE 11 Variation of Vickers hardness (H_v) as a function of B content

to be between 20.8 and 33.8 GPa for a-B_4C depending on the deposition temperature (25–900°C).[71] Accordingly, one can see that our estimation is fairly comparable with the lower limit of the experiment. For its crystalline counterpart, the reported values of 42–45 GPa[61,73,78] are slightly higher than our predictions of ~30–32 GPa. The materials beyond 70% B content have hardness, higher than 20 GPa, indicating that these disordered structures can serve as hard materials.

Pugh's ratio ($n = \mu/K$) is a method propounded by Lewandowski[79] to designate whether a material is brittle or ductile by using other mechanical properties. According to this method, if μ/K is higher (or lower) than 0.41–0.43, then material is called as brittle (or ductile). On the other way, ν can be also used to define ductile versus brittle nature of materials, and ν value is lower (higher) than 0.31–0.32 is considered to be brittle (ductile). In the last part, the Pugh ratio is calculated and presented in Figure 12. The computed Pugh ratio is in the range of 0.53–0.77, indicating that all amorphous models are brittle in nature. Besides, ν values also support this finding.

4 | DISCUSSION

a-$B_{50}C_{50}$ exhibits a mixed state of sp^2 and sp^3 hybridizations. Its sp^3/sp^2 ratio is about 61%, and hence, we believe that a-$B_{50}C_{50}$ is structurally close to the low-density amorphous diamond. Indeed, the materials up to 65% B content carry essentially the characteristic of amorphous diamond–like structure, but it is slightly softer than amorphous diamond–like structure when its mechanical properties are considered, which is probably associated with the presence of weaker B–B or B–C bonds in boron

15512916, 2023, 5, Downloaded from https://ceramics.onlinelibrary.wiley.com/doi/10.1111/jace.18979 by Abdullah Gul University, Wiley Online Library on [01/04/2024]. See the Terms and Conditions (https://onlinelibrary.wiley.com/terms-and-conditions) on Wiley Online Library for rules of use; OA articles are governed by the applicable Creative Commons License

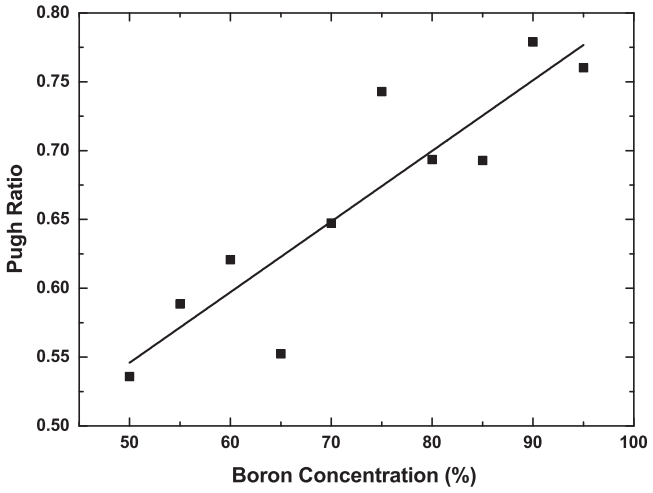

FIGURE 12 Variation of Pugh's ratio as a function of B concentration

carbides, relative to C–C bond and a low sp^3/sp^2 ratio. Because the mechanical properties amorphous diamond strongly depend on the density (or sp^3/sp^2 ratio) and increase with increasing density, high-density a-$B_{50}C_{50}$ material with different sp^3/sp^2 ratios, if they are fabricated under pressure, can show some superior properties, similar to amorphous diamond, for example, superhardness.

Beyond 65% of contents, the materials show the characteristics of both amorphous diamond and a-B because sp^3 hybridization around C atoms is still the dominant one. At 70% B content, ideal pentagonal pyramid motifs (C-B_5) develop around C atoms, and hence, the formation of $B_{11}C$ molecules is expected to occur beyond 65% B concentration. Of course, there might be some uncertainties about this composition because of the limitations in the simulations, such as timescale and size of the simulation box.

It is believed that c-B_4C consists of $B_{11}C$ icosahedrons with C—B—C intericosahedral chains rather than B_{12} icosahedrons and C—C—C linear chains.[51] It should be noted here that there exist the C—C—C (not linear chains) angles in the model up to 80% B concentration at which the motifs disappear, whereas a few C–C bonds form in a-B_4C. Consequently, a-B_4C does not have C—C—C linear chains, as proposed for its crystalline counterpart. Additionally, we witness the formation of C–B–C bond angles in the models, but we do not observe the intericosahedral linear C—B—C chains because the B—C_2 configuration does not exist in any model.

General trend in the mechanical properties of amorphous materials is to increase with increasing B content. When the amorphous and crystalline phases of materials having 10–20 C% concentrations (B/C > 4) are compared, we notice an opposite trend in the mechanical properties. Namely, the maximum hardness was observed for the stoichiometric composition (c-B_4C), and it is surprisingly decreased for nonstoichiometric B_4C (B/C > 4 or B/C < 4) compositions. For B/C > 4 materials, the decrease was explained by the substitution of the stronger B–C bonds with weaker B–B bonds. For the amorphous phases, on the other hand, we believe that the increase in the CNs and the development of more pentagonal pyramid-like topologies are probably responsible for such an increase in the mechanical properties. Note that twofold-coordination does not exist in the amorphous forms in these composition ranges but in the crystal.

Via various Vickers hardness equations, it is seen that B-rich amorphous materials beyond 70% B content have high hardness. Therefore, these materials can be referred to as hard materials. Moreover, it should be noticed that these amorphous materials show semiconducting properties, and hence, they can offer some potential applications in harsh environments.

5 | CONCLUSIONS

In the current study, for the first time, the structural, electrical, and mechanical characteristics of B-rich amorphous boron carbides (B_xC_{1-x}, $0.50 \leq x \leq 0.95$) have been analyzed by the means of ab initio MD simulations. According to the analyses, the mean CN of B atoms changes between 3.22 and 5.70, whereas that of C atoms changes from 3.46 to 4.30. The materials up to 65% B content carry essentially the characteristic of amorphous diamond, and beyond this content, the materials show the signature of both amorphous diamond and a-B because sp^3 hybridization around C atoms is still the major one in all compositions. The pentagonal pyramid motifs (C-B_5) and hence $B_{11}C$ clusters are expected to develop beyond 65% B concentration. There exist the C—C—C angles in the model up to 80% B concentration at which point they vanish. The intericosahedral linear C—B—C chains do not form because B—C_2 configuration does not occur in any model. By means of four different Vickers hardness formulas, it is found that some B-rich amorphous materials, specifically after 75% B concentration, have high Vickers hardness, and thus, they can be classified as hard materials. Although the calculated mechanical properties of amorphous boron carbides are fairly comparable with the available data of crystal and amorphous structures, we surely expect some errors in these mechanical properties because of fittings, using empirical equations, and the size of simulation cells. The HOMO–LUMO bandgap calculations expose that all amorphous configurations are semiconductors. All these conclusions are based on 200 atom amorphous configurations, but some of our findings are comparable with the

15512916, 2023, 5, Downloaded from https://ceramics.onlinelibrary.wiley.com/doi/10.1111/jace.18979 by Abdullah Gul University, Wiley Online Library on [01/04/2024]. See the Terms and Conditions (https://onlinelibrary.wiley.com/terms-and-conditions) on Wiley Online Library for rules of use; OA articles are governed by the applicable Creative Commons License

available data in the literature, and thus, we believe that these amorphous structures generated offer accurate information about the local structure of these compositions. Nevertheless, the finite size effect and the timescale of simulation cannot be ignored, and hence, additional investigations on larger systems using reliable machine learning potentials are essential to expose their microstructures and properties in detail.

ACKNOWLEDGMENTS

This research was supported by the Scientific and Technological Research Council of Turkey (TÜBİTAK) under grant number 117M372. TAY acknowledges partial financial support from YÖK 100/2000 and TÜBİTAK BİDEB 2211-C programs. The simulations were performed using the TÜBİTAK ULAKBİM-TRUBA resources.

ORCID

Murat Durandurdu https://orcid.org/0000-0001-5636-3183

REFERENCES

1. Han S, Ihm J, Louie SG, Cohen ML. Enhancement of surface hardness: boron on diamond (111). Phys Rev Lett. 1998;80(5):995.
2. Chen M, McCauley JW, Hemker KJ. Shock-induced localized amorphization in boron carbide. Science. 2003;299(5612):1563–6.
3. Wu ML, Kiely JD, Klemmer T, Hsia YT, Howard K. Process–property relationship of boron carbide thin films by magnetron sputtering. Thin Solid Films. 2004;449(1–2):120–4.
4. Jacobsohn LG, Nastasi M. Sputter-deposited boron carbide films: structural and mechanical characterization. Surf Coat Technol. 2005;200(5–6):1472–5.
5. Golikova OA. Boron and Boron-based semiconductors. Phys Status Solidi A: Appl Res. 1979;51(1):11–40.
6. Schmechel R, Werheit H. Correlation between structural defects and electronic properties of icosahedral boron-rich solids. J Phys Condens Matter. 1999;11(35):6803.
7. Thevenot F. Boron carbide—a comprehensive review. J Eur Ceram Soc. 1990;6(4):205–25.
8. Emin D. Unusual properties of icosahedral boron-rich solids. J Solid State Chem. 2006;179(9):2791–8.
9. Emin D. Icosahedral boron-rich solids as refractory semiconductors. MRS Online Proc Lib. 1987;97:3–15.
10. Zorzi JE, Perottoni CA, Da Jornada JAH. Hardness and wear resistance of B4C ceramics prepared with several additives. Mater Lett. 2005;59(23):2932–5.
11. Werheit, H. Boron-rich solids: a chance for high-efficiency high-temperature thermoelectric energy conversion. Mater Sci Eng B. 1995;29(1–3):228–32.
12. Aselage TL, Emin D, Wood C, Mackinnon I, Howard I. Anomalous Seebeck coefficient in boron carbides. MRS Online Proc Lib. 1987;97:27–32.
13. Carrard M, Emin D, Zuppiroli L. Defect clustering and self-healing of electron-irradiated boron-rich solids. Phys Rev B. 1995;51(17):11270.
14. Caruso AN, Billa RB, Balaz S, Brand, JI, Dowben PA. The heteroisomeric diode. J Phys Condens Matter. 2004;16(10): L139.
15. Ivashchenko VI, Shevchenko VI, Turchi PEA. First-principles study of the atomic and electronic structures of crystalline and amorphous B4C. Phys Rev B. 2009;80(23):235208.
16. Hong N, Mullins J, Foreman K., Adenwalla S. Boron carbide based solid state neutron detectors: the effects of bias and time constant on detection efficiency. J Phys D: Appl Phys. 2010;43(27):275101.
17. Osberg K, Schemm N, Balkir S, Brand J, Hallbeck MS, Dowben PA, et al. A handheld neutron-detection sensor system utilizing a new class of boron carbide diode. IEEE Sens J. 2006;6(6):1531–8.
18. Day E, Diaz MJ, Adenwalla S. Effect of bias on neutron detection in thin semiconducting boron carbide films. J Phys D: Appl Phys. 2006;39(14):2920.
19. Caruso AN, Dowben PA, Balkir S, Schemm N, Osberg K, Fairchild RW, et al. The all boron carbide diode neutron detector: comparison with theory. Mater Sci Eng B. 2006;135(2):129–33.
20. Domnich V, Reynaud S, Haber RA, Chhowalla M. Boron carbide: structure, properties, and stability under stress. J Am Ceram Soc. 2011;94(11):3605–28.
21. Grady DE. Hugoniot equation of state and dynamic strength of boron carbide. J Appl Phys. 2015;117(16):165904.
22. Beauvy M, Thevenot F. Le carbure de bore: matériau industriel performant. 2e partie: applications industrielles du carbure de bore. Ind Ceram. 1979;734(12):811–4.
23. Ridgway RR. Boron carbide: a new crystalline abrasive and wear-resisting product. Trans Electrochem Soc. 1934;66(1): 117.
24. Lee S, Mazurowski J, Ramseyer G, Dowben PA. Characterization of boron carbide thin films fabricated by plasma enhanced chemical vapor deposition from boranes. J Appl Phys. 1992;72(10):4925–33.
25. Kulikovsky V, Vorlicek V, Bohac P, Ctvrtlik R, Stranyanek M, Dejneka A, et al. Mechanical properties and structure of amorphous and crystalline B4C films. Diamond Relat Mater. 2009;18(1):27–33.
26. Bao R, Chrisey DB. Chemical states of carbon in amorphous boron carbide thin films deposited by radio frequency magnetron sputtering. Thin Solid Films. 2010;519(1):164–8.
27. Csákó T, Budai J, Szörényi T. Property improvement of pulsed laser deposited boron carbide films by pulse shortening. Appl Surf Sci. 2006;252(13):4707–11.
28. Kokai F, Taniwaki M, Takahashi K, Goto A, Ishihara M, Yamamoto K, et al. Laser ablation of boron carbide: thin-film deposition and plume analysis. Diamond Relat Mater. 2001;10(3–7):1412.
29. Kokai F, Taniwaki M, Ishihara M, Koga Y. Effect of laser fluence on the deposition and hardnessof boron carbide thin films. Appl Phys A. 2002;74(4):533–6.
30. Ronning C, Schwen D, Eyhusen S, Vetter U, Hofsäss H. Ion beam synthesis of boron carbide thin films. Surf Coat Technol. 2002;158:382–7.
31. Xie KY, Domnich V, Farbaniec L, Chen B, Kuwelkar K, Ma L, et al. Microstructural characterization of boron-rich boron carbide. Acta Mater. 2017;136:202–14.

15512916, 2023, 5, Downloaded from https://ceramics.onlinelibrary.wiley.com/doi/10.1111/jace.18979 by Abdullah Gul University, Wiley Online Library on [01/04/2024]. See the Terms and Conditions (https://onlinelibrary.wiley.com/terms-and-conditions) on Wiley Online Library for rules of use; OA articles are governed by the applicable Creative Commons License

32. Cheng C, Reddy KM, Hirata A, Fujita, T, Chen M. Structure and mechanical properties of boron-rich boron carbides. J Eur Ceram Soc. 2017;37(15):4514–23.
33. Chauhan A, Schaefer MC, Haber RA, Hemker KJ. Experimental observations of amorphization in stoichiometric and boron-rich boron carbide. Acta Mater. 2019;181:207–15.
34. Niihara K, Nakahira A, Hirai T. The effect of stoichiometry on mechanical properties of boron carbide. J Am Ceram Soc. 1984;67(1):C13.
35. Ishimaru M, Nakamura R, Zhang Y, Weber WJ, Peterson GG, Ianno NJ, et al. Electron diffraction radial distribution function analysis of amorphous boron carbide synthesized by ion beam irradiation and chemical vapor deposition. J Eur Ceram Soc. 2022;42(2):376–82.
36. Pallier C, Leyssale J-M, Truflandier LA, Bui AT, Weisbecker P, Gervais C, et al. Structure of an amorphous boron carbide film: an experimental and computational approach. Chem Mater. 2013;25(13):2618–29.
37. Nordell BJ, Karki S, Nguyen TD, Rulis P, Caruso AN, Purohit SS, et al. The influence of hydrogen on the chemical, mechanical, optical/electronic, and electrical transport properties of amorphous hydrogenated boron carbide. J Appl Phys. 2015;118(3):035703.
38. Nordell BJ, Nguyen TD, Caruso AN, Purohit SS, Oyler NA, Lanford WA, et al. Carbon-enriched amorphous hydrogenated boron carbide films for very-low-k interlayer dielectrics. Adv Electron Mater. 2017;3(12):1700116.
39. Soler JM, Artacho E, Gale JD, García A, Junquera J, Ordejón P, et al. The SIESTA method for ab initio order-N materials simulation. J Phys Condens Matter. 2002;14(11):2745.
40. Troullier N, Martins JL. Efficient pseudopotentials for plane-wave calculations. Phys Rev B. 1991;43(3):1993.
41. Becke AD. Density-functional exchange-energy approximation with correct asymptotic behavior. Phys Rev A. 1988;38(6):3098–100.
42. Lee C, Yang W, Parr RG. Development of the Colle-Salvetti correlation-energy formula into a functional of the electron density. Phys Rev B. 1988;37(2):785.
43. Parrinello M, Rahman A. Polymorphic transitions in single crystals: a new molecular dynamics method. J Appl Phys. 1981;52(12):7182–90.
44. Momma K, Izumi F. VESTA 3 for three-dimensional visualization of crystal, volumetric and morphology data. J Appl Crystallogr. 2011;44(6):1272–6.
45. Clark HK, Hoard JL. The crystal structure of boron carbide. J Am Ceram Soc. 1943;65(11):2115–9.
46. Krishnan S, Ansell S, Felten JJ, Volin KJ, Price DL. Structure of liquid boron. Phys Rev Lett. 1998;81(3):586.
47. Delaplane RG, Dahlborg U, Graneli B, Fischer P, Lundström T. A neutron diffraction study of amorphous boron. J Non-Cryst Solids. 1988;104(2–3):249–52.
48. Bullett DW. Structure and bonding in crystalline boron and B12C3. J Phys C: Solid State Phys. 1982;15(3):415.
49. Balakrishnarajan MM, Pancharatna PD, Hoffmann R. Structure and bonding in boron carbide: the invincibility of imperfections. New J Chem. 2007;31(4):473–85.
50. Brenner DW. Empirical potential for hydrocarbons for use in simulating the chemical vapor deposition of diamond films. Phys Rev B. 1990;42(15):9458.
51. Lazzari R, Vast N, Besson JM, Baroni S, Dal Corso A. Atomic structure and vibrational properties of icosahedral B4C boron carbide. Phys Rev Lett. 1999;83(16):3230.
52. Medvedev NN. The algorithm for three-dimensional Voronoi polyhedra. J Comput Phys. 1986;67(1):223–9.
53. Shirai K. Electronic structures and mechanical properties of boron and boron-rich crystals (Part I). J Superhard Mater. 2010;32(3):205–25.
54. Ektarawong A, Simak SI, Alling B. Effect of temperature and configurational disorder on the electronic band gap of boron carbide from first principles. Phys Rev Mater. 2018;2(10):104603.
55. Bylander DM, Kleinman L, Lee S. Self-consistent calculations of the energy bands and bonding properties of B12C3. Phy Rev B. 1990;42(2):1394.
56. Ektarawong A, Simak SI, Hultman L, Birch J, Alling B. First-principles study of configurational disorder in 4 C using a superatom-special quasirandom structure method. Phys Rev B. 2014;90(2):024204.
57. Wang H, An Q. Band-gap engineering in high-temperature boron-rich icosahedral compounds. J Phys Chem C. 2019;123(19):12505–13.
58. Sezer AO, Brand JI. Chemical vapor deposition of boron carbide. J Mater Sci Eng B. 2001;79(3):191–202.
59. Wang X, Bao ZX, Zhang YL, Li FY, Yu RC, Jin CQ. High pressure effect on structural and electrical properties of glassy carbon. J Appl Phys. 2003;93(4):1991–4.
60. Tan L, Sheng H, Lou H, Cheng B, Xuan Y, Prakapenka VB, et al. High-pressure tetrahedral amorphous carbon synthesized by compressing glassy carbon at room temperature. J Phy Chem C. 2020;124(9):5489–94.
61. Manghnani MH, Wang Y, Li F, Zinin P, Rafaniello W. Elastic and vibrational properties of B4C to 21 GPa. In: Manghnani MH, Nellis WJ, Nicol MF, editors. High pressure in science and technology. India: Universities Press; 2000. p. 945–8.
62. Emin D, Aselage T, Beckel CL, Switendick AC, Morosin B, editors. Elastic properties of boron carbides. In: Proceedings of the 10th Int. Symp. Boron, Borides and Rel. Compounds; 1990 Aug 27–30. Albuquerque, NM. New York: American Institute of Physics; 1991.
63. Aydin S, Simsek M. Hypothetically superhard boron carbide structures with a B11C icosahedron and three-atom chain. Phys Status Solidi B. 2009;246(1):62–70.
64. Shen Y, Li G, An Q. Enhanced fracture toughness of boron carbide from microalloying and nanotwinning. Scr Mater. 2019;162:306–10.
65. Aselage TL, Tallant DR, Gieske JH, Van Deusen SB, Tissot RG. Preparation and properties of icosahedral borides. In: The physics and chemistry of carbides, nitrides and borides. Dordrecht: Springer; 1990. p. 97–111.
66. Jiang C, Lin Z, Zhang J, Zhao Y. First-principles prediction of mechanical properties of gamma-boron. Appl Phys Lett. 2009;94(19):191906.
67. Jiang X, Zou JW, Reichelt K, Grünberg P. The study of mechanical properties of a-C: H films by Brillouin scattering and ultralow load indentation. J Appl Phys. 1989;66(10):4729–35.

15512916, 2023, 5, Downloaded from https://ceramics.onlinelibrary.wiley.com/doi/10.1111/jace.18979 by Abdullah Gul University, Wiley Online Library on [01/04/2024]. See the Terms and Conditions (https://onlinelibrary.wiley.com/terms-and-conditions) on Wiley Online Library for rules of use; OA articles are governed by the applicable Creative Commons License

68. Tsai JL, Tu JF. Characterizing mechanical properties of graphite using molecular dynamics simulation. Mater Des. 2010;31(1):194–9.
69. Jiang X, Reichelt K, Stritzker B. The hardness and Young's modulus of amorphous hydrogenated carbon and silicon films measured with an ultralow load indenter. J Appl Phys. 1989;66(12):5805–8.
70. Hawthorne HM. The microindentation hardness behaviour of carbon filaments, glassy carbons, and pyrolytic graphites. Carbon. 1975;13(3):215–23.
71. Kulikovsky V, Vorlicek V, Bohac P, Ctvrtlik R, Stranyanek M, Dejneka A, et al. Mechanical properties and structure of amorphous and crystalline B4C films. Diamond Relat Mater. 2009;18(1):27–33.
72. Maita JM, Song G, Colby M, Lee SW. Atomic arrangement and mechanical properties of chemical-vapor-deposited amorphous boron. Mater Des. 2020;193:108856.
73. Schwetz KA, Grellner W. The influence of carbon on the microstructure and mechanical properties of sintered boron carbide. J Less-Common Met. 1981;82:37–47.
74. Teter DM. Computational alchemy: the search for new superhard materials. MRS Bull. 1998;23(1):22–7.
75. Chen XQ, Niu H, Li D, Li Y. Modeling hardness of polycrystalline materials and bulk metallic glasses. Intermetallics. 2011;19(9):1275–81.
76. Tian Y, Xu B, Zhao Z. Microscopic theory of hardness and design of novel superhard crystals. Int J Refract Hard Met. 2012;33:93–106.
77. Jiang X, Zhao J, Wu A, Bai Y, Jiang X. Mechanical and electronic properties of B12-based ternary crystals of orthorhombic phase. J Condens Matter Phys. 2010;22(31):315503.
78. Ramana Murthy S. Elastic properties of boron carbide. J Mater Sci Lett. 1985;4(5):603–5.
79. Lewandowski JJ, Wang WH, Greer AL. Intrinsic plasticity or brittleness of metallic glasses. Philos Mag Lett. 2005;85(2):77–87.

How to cite this article: Yıldız TA, Durandurdu M. Ab initio study of boron-rich amorphous boron carbides. J Am Ceram Soc. 2023;106:2862–2874. https://doi.org/10.1111/jace.18979

15512916, 2023, 5, Downloaded from https://ceramics.onlinelibrary.wiley.com/doi/10.1111/jace.18979 by Abdullah Gul University, Wiley Online Library on [01/04/2024]. See the Terms and Conditions (https://onlinelibrary.wiley.com/terms-and-conditions) on Wiley Online Library for rules of use; OA articles are governed by the applicable Creative Commons License